

An Enhanced AUSM⁺-up Scheme for High-Speed Compressible Two-Phase Flows on Hybrid Grids

A. K. Pandare*, H. Luo* and J. Bakosi**
Corresponding author: hong_luo@ncsu.edu

* Department of Mechanical and Aerospace Engineering,
North Carolina State University, Raleigh, NC, 27695, USA.

** Computational Physics Group (CCS-2),
Computer, Computational and Statistical Sciences Division,
Los Alamos National Laboratory, Los Alamos, NM 87545, USA.

Abstract: An enhanced AUSM⁺-up scheme is presented for high-speed compressible two-phase flows using a 6-equation two-fluid single pressure model. Based on the observation that the AUSM⁺-up flux function does not take into account relative velocity between the two-phases, and thus is not stable and robust for computation of two-phase flows involving interaction of strong shock waves and material interfaces, the enhancement is in the form of a volume-fraction coupling term and a modification of the velocity-diffusion term, both proportional to the relative velocity between the two-phases. These modifications in the flux function obviate the need to employ the exact Riemann solver, leading to a significantly less expensive yet robust flux scheme. Furthermore, the hyperbolic tangent interface capturing (THINC) scheme is used in order to provide a sharp resolution for material interfaces. A number of benchmark test cases are presented to assess the performance and robustness of the enhanced AUSM⁺-up scheme for compressible two-phase flows on hybrid unstructured grids. The numerical experiments demonstrate that the enhanced AUSM⁺-up scheme along with THINC scheme can efficiently compute high-speed two-fluid flows such as shock-bubble interactions, while accurately capturing material interfaces.

Keywords: Two-fluid model, Shock waves, Material interfaces, AUSM

1 Introduction

Separated two-phase flows arise in a myriad of engineering applications such as cavitation, underwater explosion, atomization of fuel droplets, departure from nucleate boiling in reactors, etc. Modeling and simulation of these multiphase flows is an invaluable tool to study and understand such flows. The two types of methods used to model multiphase flows are interface tracking and interface capturing methods. Interface tracking methods, as the name suggests, employ actual tracking of the interface between two phases (viz. bubble or droplet surfaces) and smoothing the fluid properties across this interface. The level-set, volume-of-fluid, front-tracking and Lagrangian tracking are some famous interface tracking methods. Interface capturing methods, on the other hand, dynamically “capture” the interfaces; just like a standard finite-volume or discontinuous Galerkin method would capture shocks and contact discontinuities without any special treatment. This means that each phase is treated as a separate continuum, and that there is no clear distinction between cells containing one phase or the other. Each cell contains a fraction of each phase, denoted by the volume fraction α . This approach is thus also termed as the “interpenetrating continua” approach, or the diffuse interface method (DIM).

The equations for the DIM are derived from individual continuum equations for each phase, called the local instant formulation; and then applying an averaging procedure [1]. The result is 6 equations: continuity, momentum and total energy equations for each phase. This two-fluid system is incomplete due to more

unknowns than the number of equations. Various approaches to close the system exist. One of these is to adopt a single-pressure assumption leading to the Wallis model [2]. This leads to the 6-equation model of two-fluid flow. This model has been used to simulate inviscid two-fluid flow first by Toumi [3] and then by Chang, Liou and co-workers [4, 5, 6, 7]. Niu [8, 9] has used a primitive variable solver to improve upon this method. Other approaches to solve two-phase flows using the Wallis model include work by Dinh et al. [10] and Nourgaliev et al. [11] Vazquez-Gonzalez et al. [12] study the necessity of hyperbolization of this model and compare results of an elliptic solver with the hyperbolic methods mentioned above. Another approach to close the incomplete DIM two-fluid system is by including an additional equation for volume fraction. This additional equation leads to a 7-equation two-pressure system [13], which is hyperbolic. This model was used by Saurel et al. [14, 15, 16], and improved upon in a following work [17]. The 7-equation model allows non-equilibrium of phasic pressures, velocities and internal energies, which relaxes the pressure equilibrium assumption of the single pressure model.

In this work, the two-fluid single pressure model is used, and the focus is on shock-bubble interaction problems. Severe two-phase flow problems such as shock-interface interactions pose a challenge for multiphase methods, in the sense of maintaining robustness and stability. This requires well-designed discretizations of the inviscid fluxes. In context of the two-fluid model, relative velocities reach extremely large values in the regions of shock-interface interactions. It is known that FVS schemes in their standard forms predict negative pressures in these zones, resulting in failure of the computation [18, 6]. The current state of practice was proposed by Chang and Liou [4]. Their solution was to augment the FVS scheme, such as AUSM⁺-up [19], with an exact Riemann solver at interfaces. This results in a robust flux scheme, able to retain pressure positivity in the regions in question. However, there are two difficulties in this:

1. The stratified-flow model has to be applied to “split” the flux into the FVS and exact-Riemann parts, which is complicated to visualize and implement in multi dimensions.
2. The exact Riemann solver becomes very expensive in regions where strong shocks interact with material interfaces. This is because the solver requires a large number of Newton iterations to get a correct middle-zone pressure p^* in these regions.

Thus, although the resulting Godunov+AUSM⁺ method is robust, it comes at a large computational cost and implementation complexity. The computational costs have been studied by Kitamura and Nonomura [18]. It has been observed that, it is in these regions of extremely high relative velocities between the phases, where the standard FVS schemes such as AUSM⁺-up break down due to negative pressure predictions. This begs the question: do the eigenvalues of the two-fluid system (which do not have a closed-form expression) have a dependence on the relative velocity? This is the foundation of enhancement in the AUSM⁺-up fluxes proposed in this work. It builds on the initial modification in the granular mass-fluxes by Houim and Oran [20], which was used successfully by Pandare and Luo [21, 22] in the context of two-fluid flows. This modification involves a volume-fraction coupling term in the mass-flux. In addition to that a further modification in the velocity-diffusion term in the pressure flux is proposed, which imparts additional stability to the scheme. The resulting flux is termed as the AUSM⁺-upf flux. This work studies some severe shock-interface interaction problems which cannot be otherwise simulated using the AUSM⁺-up flux alone, in addition to other such shocked two-phase problems. It can also be proven easily that this choice of flux, coupled with an appropriate discretization of the pressure flux and other non-conservative terms, satisfies the pressure non-disturbance condition (also known as Abgrall’s criterion [23, 15] or well-balancedness [24]), which is essential for the solver to maintain a stationary contact discontinuity.

The diffuse interface method, as the name suggests, smears out material interfaces, sometimes beyond recognition. However, the cost effectiveness of the DIM makes it a more desirable multiphase simulation tool than interface-tracking methods in many situations. Thus, significant research has been directed at “sharpening” these diffuse interfaces. The reconstruction of the volume-fraction derivatives is key in this respect. Limiting the reconstructed derivatives correctly has been proven to significantly improve the interface capturing capabilities of the DIM. One of such methods is the hyperbolic tangent interface capturing (THINC) method [25, 26], which assumes a hyperbolic tangent distribution of the volume fraction over each mesh-cell and uses this to obtain reconstructed volume fractions to compute numerical fluxes. Another approach is the Overbee limiter [27] which modifies the Superbee limiter to be less restrictive and sharply capture the material interface. Needless to say, both these limiters are applied only to the volume fraction and not to the flow variable. In this work the THINC scheme is used to sharpen the interfaces.

The rest of the article is organized as follows: the governing equations of the two-fluid model and closure laws are discussed in the next section. This is followed by a description of the spatial and temporal discretization and other numerics. This section discusses the enhancements made in the AUSM⁺-up fluxes and the limiting process used for interface sharpening. The results obtained using the proposed modifications are presented next. The problems in focus are tests that involve strong shock and material interface interactions. The importance of interface sharpening is discussed in this section. This is followed by concluding remarks.

2 Governing Equations

2.1 The two-fluid model

The two-fluid model uses the interpenetrating continua approach to model two-phase flows. This model requires an averaging procedure to filter-out the local instantaneous fluctuations very similar to the Reynolds' averaging in turbulence. Interphasic mass-transfer terms have not been considered in this work. The resulting two-fluid model given by Ishii [1] and concisely by Staedtke [28], using k as the index for the two fluids, is as follows:

$$\frac{\partial \mathbf{U}_k}{\partial t} + \frac{\partial \mathbf{F}_{k_j}}{\partial x_j} = \mathbf{P}_k^{int} + \mathbf{S}_k \quad (1)$$

where,

$$\mathbf{U}_k = \begin{bmatrix} \alpha_k \rho_k \\ \alpha_k \rho_k u_{k_i} \\ \alpha_k \rho_k E_k \end{bmatrix} \quad (2)$$

$$\mathbf{F}_{k_j} = \begin{bmatrix} \alpha_k \rho_k u_{k_j} \\ \alpha_k \rho_k u_{k_i} u_{k_j} \\ \alpha_k \rho_k u_{k_j} H_k \end{bmatrix} + \begin{bmatrix} 0 \\ \alpha_k p \delta_{ij} \\ 0 \end{bmatrix} \quad (3)$$

$$\mathbf{P}_k^{int} = \begin{bmatrix} 0 \\ p_k^{int} \frac{\partial \alpha_k}{\partial x_i} \\ -p_k^{int} \frac{\partial \alpha_k}{\partial t} \end{bmatrix} \quad k = 1, 2. \quad (4)$$

\mathbf{S}_k represent source terms, for example due to phase transitions and body forces.

The system (1) has 11 unknowns ($\alpha_k, \rho_k, u_k, E_k, p_k^{int}, p$ with $k = 1, 2$) and a total of 9 equations with 6 PDEs, 2 equations of state (EoS) and the constraint on volume fractions,

$$\sum_{k=1}^2 \alpha_k = 1. \quad (5)$$

These equations constitute the Wallis two-fluid model or the 6-equation single-pressure model of two-phase flows. The EoS required to close this system are given in the next subsection. Another condition that the interfacial pressures should cancel each other if no other stresses such as surface tension are considered at the interface gives,

$$p_g^{int} = p_l^{int} \equiv p^{int}. \quad (6)$$

p^{int} is explicitly given as a function of the other unknowns. Here, we use the relation given by Stuhmiller [29],

$$p^{int} = p - \sigma \frac{\alpha_g \alpha_l \rho_g \rho_l}{\alpha_g \rho_l + \alpha_l \rho_g} u_r^2 \quad (7)$$

where $u_r = |u_l - u_g|$. This interface pressure term helps restore hyperbolicity to the system [5]. This provides the additional 3 equations and the system of equations is closed. The effect of addition of the interface pressure term has been analyzed in detail by Chang et al. [30]. They show that there is a limiting value of σ above which the system (1) is hyperbolic. Here, a value of $\sigma = 2$ is used for all the problems.

2.2 Equations of state

The stiffened-gas equations of state (*SG-EoS*) are used for each fluid in this work. Using the *SG-EoS*, the pressure, temperature and speed of sound are given respectively as:

$$\rho E_k = \frac{p + P_{c_k}}{\gamma_k - 1} + \frac{\rho \mathbf{u}_k^2}{2} + P_{c_k} \quad (8)$$

$$T_k = \left(\frac{\gamma_k}{\gamma_k - 1} \right) \frac{(p + P_{c_k})}{\rho_k C_{p_k}} \quad (9)$$

$$a_k = \sqrt{\gamma_k \frac{p + P_{c_k}}{\rho_k}}. \quad (10)$$

Ideal gas values are used for air whereas the following properties are used for water:

$$\begin{aligned} \gamma_l &= 2.8 \\ P_{c_l} &= 8.5 \times 10^8 \text{ Pa} \\ C_{p_l} &= 4186.0 \text{ J/(kg} \cdot \text{K)}, \end{aligned}$$

for Helium:

$$\begin{aligned} \gamma_{He} &= 1.648 \\ P_{c_{He}} &= 0.0 \text{ Pa} \\ C_{p_{He}} &= 5192.6 \text{ J/(kg} \cdot \text{K)}, \end{aligned}$$

and for the R-22 refrigerant:

$$\begin{aligned} \gamma_{R22} &= 1.249 \\ P_{c_{R22}} &= 0.0 \text{ Pa} \\ C_{p_{R22}} &= 456.0 \text{ J/(kg} \cdot \text{K)}. \end{aligned}$$

3 Spatial discretization

The two-fluid system (1) is discretized using a second-order finite volume method. On integrating over each element e , and applying the divergence theorem on the flux terms, the discrete system becomes,

$$\int_{\Omega_e} \frac{\partial \mathbf{U}_k}{\partial t} d\Omega + \int_{\Gamma_e} (\mathbf{F}_k \cdot \mathbf{n}) d\Gamma = \int_{\Omega_e} (\mathbf{P}_k^{int} + \mathbf{S}_k) d\Omega. \quad (11)$$

Here, the cells are denoted by Ω_e and the cell-faces by Γ_e . A least-squares reconstruction procedure is used on the primitive variables to obtain second order. The primitive variables chosen here are

$$\mathbf{V} = [T_1 \quad u_1 \quad T_2 \quad u_2 \quad p \quad \alpha_1]^T. \quad (12)$$

A vertex-based limiter (VB) proposed by Kuzmin [31] is used to suppress the spurious oscillations in the flow field, when discontinuities are expected. The diffused interface method is known to smear material interfaces. To be able to capture these interfaces sharply, the Hyperbolic Tangent Interface Capturing (THINC) scheme [25, 26] is used. The THINC scheme is now discussed briefly; followed by discretization of each term in this system is now individually discussed.

3.1 Interface sharpening using the THINC scheme

The THINC scheme has previously been used by Kitamura et al. [32] for sharp interface capturing with the two-fluid model. However, in their work, a one-dimensional approach was used on a structured mesh

to obtain the sharpened interface. Here, the multidimensional THINC [26] is used. This allows its use on unstructured meshes. The THINC scheme is essentially a way to limit the derivatives of the volume-fraction in the vicinity of material interfaces. Using the VB limiter on these causes extremely diffused interfaces. However, it has been observed that it is necessary to use THINC only in appropriate regions [32] where $\chi\epsilon < \alpha < 1 - \chi\epsilon$. In other single-phase dominated regions, using THINC causes non-monotonic void-fraction distributions. Here, χ is set to 2 and ϵ is the minimum value of volume fraction permitted, which is set to 10^{-5} unless otherwise stated in the problem definition. Also, in the vicinity of interfaces, velocity and pressure gradients are set to zero, as suggested by Chiapolino et al. [27]. This region is determined by:

$$\alpha_1\alpha_2 > 10^{-2}.$$

This ensures stable interfaces, which otherwise would be affected by limiter interactions (VB and THINC in this case). Note that the temperature gradients are kept unchanged in this region. Also note that everywhere else in the domain, the VB limiter is used for all flow variables without modifications. Thus, it is only in the regions where $\chi\epsilon < \alpha < 1 - \chi\epsilon$ that the volume-fraction is limited using THINC.

The THINC scheme approximates the volume-fraction distribution near interfaces by the hyperbolic tangent function. The step-like nature of the tanh function facilitates sharp interface-capturing of interfaces. In this work, we use the multidimensional THINC, for which the volume-fraction in a cell- i near the interface is approximated by,

$$\alpha_i(\xi, \eta) = \frac{1}{2} (1 + \tanh(\beta(\mathcal{P}_i + d_i))), \quad (13)$$

where,

$$\mathcal{P}_i(\xi, \eta) + d_i = 0 \quad (14)$$

is the equation of the interface and β is a parameter that controls the sharpness of the interfaces. The mapping to reference coordinates $(x, y) \rightarrow (\xi, \eta)$ can be facilitated using the elemental shape functions [26, 33]. The order polynomial \mathcal{P}_i can be chosen to represent the material interface in a piecewise manner over each cell. Here, a linear approximation is chosen for the interface equation:

$$a_\xi\xi + a_\eta\eta + d_i = 0. \quad (15)$$

Here, a_ξ and a_η are derivatives of the volume-fraction in the reference coordinate system. d_i can be found using the fact that,

$$\overline{\alpha}_i = \frac{1}{\Omega_i} \int_{\Omega_i} (a_\xi\xi + a_\eta\eta + d_i) d\Omega. \quad (16)$$

Details are underlined in the appendices of the references [26, 33]. Using Eq. 13 the volume-fraction is reconstructed to the face-centers when fluxes are to be computed.

Effects of using the THINC scheme on interfaces are outlined in the results section. It should be noted here that the parameter β is set to 2 for all the test problems in this work. The inviscid fluxes are now discussed in detail.

3.2 Inviscid fluxes

Inviscid fluxes in the two-fluid model can be discretized using two types of numerical fluxes as described by Kitamura et al. [6]:

1. AUSM-family standalone: The all-speed variant AUSM⁺-up developed by Liou [19] and extended to the stratified-flow two-fluid model in [5] is employed in this type. A single flux-function is used to compute the flux at the cell-interfaces.
2. Hybrid AUSM+Riemann (Godunov) solver: Flux at the cell-interface is split into fluxes between *like* phases (l - l , g - g) and *unlike* phases (l - g , g - l). Naturally, this type of split-flux treatment requires a

stratified flow assumption. Fluxes between *like* phases are computed using the AUSM⁺-up scheme and those between *unlike* phases are computed using the Godunov method [4]. This approach is expensive since the Godunov method uses iterations to accurately predict the fluxes.

These two types of flux schemes have been studied in detail by Kitamura et al. [6] where it has been noted that a hybrid scheme is necessary for situations where a strong pressure discontinuity interacts with a void-fraction discontinuity. A high pressure-ratio water-air shocktube, a shock/water-column interaction and a shock/air-bubble interaction have been used to illustrate this. However, in this work, a modification to the AUSM⁺-up flux is used, which makes it possible to solve the above mentioned problems. The new scheme involves an additional coupling between the mass-flux and the volume-fraction of the dispersed phase. In addition to that the velocity-diffusion term in the pressure flux is modified in a manner appropriate for usage in the two-fluid model discretization. The AUSM⁺-up flux with these modifications is referred to as the AUSM⁺-upf in this work; where the f stands for the volume-fraction coupling.

The AUSM⁺-up flux developed by Liou [19] specifically for all-speed application is a wise choice for two-fluid problems. In the AUSM-type of flux methods, the fluxes are written as,

$$\mathcal{F}_{k,L/R} = \dot{m}_{k,1/2} \boldsymbol{\psi}_{k,1/2} + \alpha_{k,L/R} p_{k,1/2} \mathbf{n}_{1/2}. \quad (17)$$

Please note here that although the pressure flux $p_{k,1/2}$ contributes differently to the two phases $k = 1, 2$, the pressure of the two phases p is equal. $\boldsymbol{\psi}_{k,1/2} = (1, u, H)_{k,1/2}^T$ is upwinded in the standard way,

$$\boldsymbol{\psi}_{k,1/2} = \begin{cases} \boldsymbol{\psi}_{k,L} & \text{if } \dot{m}_{k,1/2} > 0 \\ \boldsymbol{\psi}_{k,R} & \text{otherwise.} \end{cases} \quad (18)$$

Note that the pressure flux contribution to the left and right elements is different due to the difference in the volume fractions at the face: $\alpha_{k,L} \neq \alpha_{k,R}$. The mass flux and the Mach number of phase- k is given as,

$$\dot{m}_{k,1/2} = M_{k,1/2} a_c \begin{cases} \alpha_{k,L} \rho_{k,L} & \text{if } M_{k,1/2} > 0, \\ \alpha_{k,R} \rho_{k,R} & \text{otherwise,} \end{cases} \quad (19)$$

$$M_{k,1/2} = \mathcal{M}_{(4)}^+(M_{k,L}) + \mathcal{M}_{(4)}^-(M_{k,R}) + M_{k,p}, \quad (20)$$

where the split Mach numbers $M_{(m)}^\pm$ are,

$$\mathcal{M}_{(1)}^\pm(M) = \frac{1}{2}(M \pm |M|), \quad (21)$$

$$\mathcal{M}_{(2)}^\pm(M) = \frac{1}{4}(M \pm 1)^2, \quad (22)$$

$$\mathcal{M}_{(4)}^\pm(M) = \begin{cases} \mathcal{M}_{(1)}^\pm(M) & \text{if } |M| \geq 1, \\ \mathcal{M}_{(2)}^\pm(M)(1 \mp 2\mathcal{M}_{(2)}^\mp(M)) & \text{otherwise,} \end{cases} \quad (23)$$

the Mach numbers are defined as,

$$M_{k,L/R} = \frac{u_{k,L/R}}{a_c}. \quad (24)$$

and the common speed of sound given by Chang and Liou [4] is used:

$$\frac{1}{a_c} \left(\frac{\alpha_1}{\rho_1} + \frac{\alpha_2}{\rho_2} \right) = \frac{\alpha_1}{\rho_1 a_1^2} + \frac{\alpha_2}{\rho_2 a_2^2}. \quad (25)$$

The pressure diffusion term $M_{k,p}$ introduced to treat low Mach number flows is,

$$M_{k,p} = -K_p \max(1 - \overline{M}_k^2, 0) \frac{p_R - p_L}{\rho_{k,1/2} a_c^2}, \quad (26)$$

$$\overline{M}_k^2 = \frac{u_{k,L}^2 + u_{k,R}^2}{2a_c^2}. \quad (27)$$

The subscript ‘1/2’ has been used for definitions of a and ρ to represent averages of the left and right states. This term is especially important for the two-fluid system where the stiffened gas equation is used.

The pressure flux is given as,

$$p_{k,1/2} = \mathcal{P}_{(5)}^+(M_{k,L})p_L + \mathcal{P}_{(5)}^-(M_{k,R})p_R + p_{k,u}, \quad (28)$$

where the split Mach numbers for pressure are,

$$\mathcal{P}_{(5)}^\pm(M) = \begin{cases} \frac{1}{M} \mathcal{M}_{(1)}^\pm & \text{if } |M| \geq 1, \\ \frac{1}{M} \mathcal{M}_{(2)}^\pm [(\pm 2 - M) \mp 3M \mathcal{M}_{(2)}^\mp] & \text{otherwise.} \end{cases} \quad (29)$$

The velocity diffusion $p_{k,u}$ is then defined as,

$$p_{k,u} = -K_u \mathcal{P}_{(5)}^+(M_{k,L}) \mathcal{P}_{(5)}^-(M_{k,R}) \cdot (\rho_{k,1/2} a_c) (u_{k,R} - u_{k,L}). \quad (30)$$

This choice of fluxes yielded a stable scheme for most of the cases presented. However, for some extreme cases, such as the high pressure-ratio water-air shocktube, shock-watercolumn and shock-bubble interaction and the very low Mach number channel flows, it was observed that a small amount of dissipation in the mass-fluxes was necessary to obtain stability in regions of high relative velocities.

Note that the two-fluid model with equal phase velocities and pressure, known as the homogeneous two-phase model, is hyperbolic in nature. The Wallis model, which doesn’t assume this however, is non-hyperbolic in its original form [28]. It is surmised that when the relative velocities increase to high values, the stratified fluid model tends more to the non-hyperbolic nature and the hyperbolic correction (7) proves to be insufficient to ensure real eigenvalues. The fact that this correction is insufficient to completely eliminate the nonhyperbolic nature at all physically admissible states has been noted by Hérard et al. [34, 35].

Note here that in spite of adding the hyperbolic correction term, the explicit eigen-structure (and hence the exact acoustic speed) for this system is unknown. There is a possibility that, in assuming that the system acoustic speed as a function of the acoustic speeds of the two individual phases alone, a possible effect of relative velocities on the acoustic properties of the system is being neglected. Liou and Edwards [36] have investigated the importance of using the appropriate speed of sound in the numerical fluxes. If there is a possible dependence of the speed of sound on the relative velocity, a dissipation term proportional to the relative velocity of the two-phases, would stabilize the discretization. The dissipation needs to be in the form of an additional coupling between the mass-flux and the volume-fraction. This approach has been utilized by Houim and Oran [20] in case of granular two-fluid flows. A similar form of the dissipation term has been utilized in this work. The modified mass flux is given as,

$$\dot{m}_{k,1/2} = M_{k,1/2} a_c \alpha_k \rho_k - \mathcal{D}_{k,f}, \quad (31)$$

where \mathcal{D}_f is the volume-fraction coupling term,

$$\mathcal{D}_f = \frac{1}{2} \lambda_r \frac{\max(\alpha_L, \alpha_R)}{\alpha_{crit}} (\alpha_R \rho_R - \alpha_L \rho_L), \quad (32)$$

where the phase subscripts are omitted, and the maximum normal relative velocity is,

$$\lambda_r = \max(u_{r,L}, u_{r,R}), \quad (33)$$

$$u_r = \mathbf{U}_r \cdot \mathbf{n}. \quad (34)$$

Clearly, the relative velocity λ_r is taken into consideration via this coupling term. Note that although this term derives its true form from the Lax-Friedrichs flux, unlike the latter, it is well-balanced in nature. This means that it satisfies Abgrall’s criterion [15], also known as the pressure non-disturbance condition [4]. Another way to stabilize this model is increasing the drag coefficient, resulting in an absolute velocity relaxation. This way, although found to be effective, might yield unphysical results and this assumption is not valid for applications targeted here. Hence we resort to the volume-fraction coupling for stability purposes. The importance of using the correct speed of sound for the system in the calculations of Mach number and dissipation terms for the inviscid flux scheme has also been highlighted by Liou and Edwards [36].

Additionally, it has been observed [18] that the AUSM⁺-up fluxes lead to negative pressure-fluxes in regions where strong-shocks interact with material discontinuities. The cause of this negative pressure-flux in Eq. (28) in spite of positive p_L and p_R is the all-speed pressure-flux correction $p_{k,u}$ from Eq. (30). This pressure-velocity coupling term becomes too large due to the large value of a_c and causes negative $p_{k,1/2}$. Here, it is replaced by

$$\tilde{p}_{k,u} = -K_u \left(1 - \mathcal{P}_{(5)}^+(M_{k,L}) \mathcal{P}_{(5)}^-(M_{k,R}) \right) \cdot (\rho_{k,1/2} \lambda_r) (u_{k,R} - u_{k,L}). \quad (35)$$

Note how the behavior of this term has been inverted such that as the Mach number reaches 0, $\tilde{p}_{k,u}$ also reaches 0; as against the typical $p_{k,u}$ from Eq. (30), which reaches 0 at Mach number 1. This is done so that the effect of this term is more pronounced at high Mach numbers, i.e. strong shocks, which is where the standard AUSM⁺-up flux tends to fail. The modified AUSM⁺-up flux is referred to as the AUSM⁺-up flux henceforth.

These modifications ensure the positivity of pressure-flux when the left and right side pressures p_L and p_R are positive. The rationale for deriving the form of these terms is inspired from works of Liou [19] and Edwards [37]. The effects of these additional terms can be seen for high pressure ratio shocks as encountered in the water-air shocktube and the shock-bubble interaction problems. These problems cannot be solved without the aforementioned dissipative terms accounted for, as also reported by Kitamura et al. [6]. Various other ways have also been used to solve this issue. Chang and Liou [4] use an exact Riemann solution in the region $|\alpha_{1,L} - \alpha_{1,R}|$. This model although robust, turns out to be quite expensive since a Newton iteration is required to solve for the pressure in this region. Also, the full eigenstructure of the system needs to be known for this method. Kitamura et al. [18] use an HLLC flux in this region to replace the exact Riemann solver used by Chang and Liou. The HLLC flux, albeit more economical than the exact Riemann solver, still requires knowledge of the eigenstructure of the system. The modifications proposed here do not require this, and could potentially be used for other types of equations of state. A detailed discussion of the effects of the proposed modifications will be provided in the numerical results section.

3.3 Non-conservative spatial derivative

The term \mathbf{P}^{int} is comprised of non-conservative first derivatives in space and time. This necessitates the use of so-called “well-balanced” discretizations. Extensive studies of well-balanced discretizations of non-conservative PDEs have been done, starting from Pares’ work [24], leading to Roe-type [38] and Osher-type [39] schemes for these equations. A numerical method for the two-fluid equations specifically was also proposed based on this concept [40]. This collection of work clearly states that the well-balancedness is an essential property to be considered while designing a numerical method for solving non-conservative PDEs, to maintain global conservation. Abgrall, in one of his early works [23], also focuses on this property in the context of multi-species (or multi-component) equations.

Consider a domain Ω with boundaries Γ . The pressure flux $\alpha_k \nabla p$ on this domain can be simply written as,

$$\int_{\Omega} \alpha_k \frac{\partial p}{\partial x_i} d\Omega.$$

Consider now, an element Ω_e a part of the triangulation of Ω . Since this term is non-conservative, it is not clear how this term should be discretized in this form. Thus, using integration-by-parts, this term can be

expanded on the element Ω_e as,

$$\int_{\Omega_e} \alpha_k \frac{\partial p}{\partial x_i} d\Omega = \int_{\Gamma_e} \alpha_k p n_i d\Gamma - \int_{\Omega_e} p \frac{\partial \alpha_k}{\partial x_i} d\Omega,$$

where n_i is the i -component of the normal to the element boundary Γ_e , pointing outward of Ω_e . Now, the first term is an integral over the cell-boundary Γ_e which uses the value of the integrand ($\alpha_k p$) from the cell Ω_e . This term takes into account the jump of the function at each cell-boundary. The pressure for this term should be obtained by the Riemann solver used (AUSM⁺-upf in this case, $p_{k,1/2}$) since otherwise it is not uniquely defined on the cell-boundary. On the other hand, the volume-fraction for this term is supposed to be reconstructed from the cell Ω_e . Thus, on each cell-boundary, this term will have a different contribution to the cells straddling the boundary only due to the volume-fraction α_k in it. This first term corresponds to the pressure flux part in Eq. (17). The second term can be treated as a source term since it is an integral over the cell Ω_e only. This clearly shows that the non-conservative term has non-unique values at the element faces, one from each side of the face. This type of treatment ensures the well-balanced nature of the discretization. Thus, the ‘‘stratified-flow model’’ discretization of the nonconservative term [4] is obtained by applying integration-by-parts to the pressure term in the two-fluid model while writing it in the discrete form.

The non-conservative time derivative term is combined with the time-derivative of the unknowns which modifies \mathbf{U} . This will be discussed in the following section pertaining to time integration. Interface momentum transfer and other source terms \mathbf{M}_k and \mathbf{S}_k are treated as volume-averaged source terms.

4 Time integration

Before discretizing the time derivative term $\frac{\partial \mathbf{U}}{\partial t}$, the non-conservative time derivative term in \mathbf{P}^{int} has to be combined into the vector of unknowns \mathbf{U} . This results in a modified vector of unknowns for fluid k ,

$$\hat{\mathbf{U}}_k = \mathbf{U}_k + \begin{bmatrix} 0 \\ 0 \\ p^{int} \alpha_k \end{bmatrix}. \quad (36)$$

This results in the final form of the semi-discrete form of the two-fluid system:

$$V \frac{\partial \hat{\mathbf{U}}}{\partial t} = \mathcal{R}, \quad (37)$$

where V is the cell-volume. The discretized right-hand side vector \mathcal{R} and the modified unknown vector $\hat{\mathbf{U}}$ are,

$$\mathcal{R} = -\mathcal{F} + \mathcal{G} + \hat{\mathcal{P}}^{int} + \mathcal{S}, \quad \hat{\mathbf{U}} = \begin{bmatrix} \alpha_1 \rho_1 \\ \alpha_1 \rho_1 u_{1_i} \\ \alpha_1 \rho_1 E_1 + p^{int} \alpha_1 \\ \alpha_2 \rho_2 \\ \alpha_2 \rho_2 u_{2_i} \\ \alpha_2 \rho_2 E_2 + p^{int} \alpha_2 \end{bmatrix}, \quad (38)$$

where,

$$\mathcal{S} = \int_{\Omega_e} \mathbf{S} d\Omega, \quad \hat{\mathcal{P}}^{int} = \begin{bmatrix} 0 \\ \int_{\Omega_e} p^{int} \frac{\partial \alpha_1}{\partial x_i} d\Omega \\ 0 \\ 0 \\ \int_{\Omega_e} p^{int} \frac{\partial \alpha_2}{\partial x_i} d\Omega \\ 0 \end{bmatrix}. \quad (39)$$

The system of equations (37) is integrated in time to obtain a time-marching scheme.

In this work, the explicit 3-stage third order TVD Runge-Kutta (RK3) scheme [41] has been used to integrate the system (37) in time. The explicit TVDRK3 is straight-forward to apply to the two-fluid system, and implementation details can be found in [6].

4.1 Decoding of pressure and volume fractions

The TVDRK3 method works with the conservative variables $\hat{\mathbf{U}}$. Once the new vector of unknowns $\hat{\mathbf{U}}^{n+1}$ is obtained, it is necessary to obtain the pressure and volume fractions at time-step $n + 1$. The decoding procedure highlighted by Liou and coworkers [4, 6], is used for this purpose. Imposing the constraint on the volume fraction (5) and the two *EoS*, the quadratic equation for p^{n+1} is obtained,

$$p^2 - Bp - C = 0, \quad (40)$$

with the positive root,

$$p = \frac{1}{2} \left(B + \sqrt{B^2 + 4C} \right) \quad (41)$$

and the volume fraction is given by,

$$\alpha_k = \frac{\hat{A}_k}{p + \hat{a}_k}, \quad (42)$$

where,

$$\hat{A}_k = (\gamma_k - 1) \left(\hat{\mathbf{U}}_{3,k} - \frac{|\hat{\mathbf{U}}_{2,k}|^2}{2\hat{\mathbf{U}}_{1,k}} \right), \quad (43)$$

$$\hat{a}_k = \gamma_k P_{c_k} + (\gamma_k - 1)p^{int}, \quad (44)$$

$$B = \sum_{k=1}^2 (\hat{A}_k - \hat{a}_k), \quad (45)$$

$$C = \hat{a}_1 \hat{A}_2 + \hat{a}_2 \hat{A}_1 - \hat{a}_1 \hat{a}_2. \quad (46)$$

The numerical errors in computation of p and α_k can be very large, considering the large values of P_{c_k} . A Newton iteration procedure is used to reduce these errors, by solving (43) for both the phases simultaneously:

$$(p + \hat{a}_g) \alpha_g - \hat{A}_g = 0, \quad (47)$$

$$(p + \hat{a}_l) \alpha_l - \hat{A}_l = 0. \quad (48)$$

Typically, a few iterations are enough to drive the pressure error below 10^{-6} .

4.2 Treatment for vanishing phase: blending

A matter of concern while solving Eq. (37) is that of phase disappearance. In this situation, the numerical errors in the solution get amplified due to the division by a very small volume fraction. Although the volume of the corresponding fluid and thus its contribution to the flow are negligible, the calculation procedure might become unstable due to unrealistic values of the flow variables, leading to divergence. The idea of the blending function suggested by Paillère et al. [42] is employed to suppress these numerical errors. It is assumed that when a fluid nears phase-disappearance, the fluids reach equilibrium immediately by mixing their states. After the time-integration and decoding procedure, if $\epsilon_{min} \leq \alpha_k \leq \epsilon_{max}$, then the velocity and

temperature fields of phase- k are blended using,

$$u_k|_{blended} = G(\psi_k)u_k + (1 - G(\psi_k))u_k'. \quad (49)$$

The function $G(\psi)$, $\psi \in [0, 1]$, is a cubic polynomial interpolant with $G(0) = 0$, $G(1) = 1$ and $G'(0) = G'(1) = 0$. The function,

$$G(\psi) = -\psi^2(2\psi - 3) \quad (50)$$

is used here, where ψ is the normalized volume fraction,

$$\psi = \frac{\alpha - \epsilon_{min}}{\epsilon_{max} - \epsilon_{min}}. \quad (51)$$

The parameters ϵ define the range of volume fractions within which blending is employed. They are preset as,

$$\epsilon_{min} = 10^{-1}\epsilon \quad (52)$$

$$\epsilon_{max} = 10^3\epsilon, \quad (53)$$

where ϵ is problem specific, but usually is set at 10^{-7} .

5 Results

This section validates the discretization and flux-scheme for the two-fluid single pressure model presented in the previous sections. Several test problems from previous work by Nonomura et al. [32] and Haimovich and Frankel [43] have been considered for validation purposes. The purpose of this section is two-fold: Validation of the enhancements to the AUSM⁺-up flux, and demonstrating the interface sharpening capabilities of the THINC scheme. It should be noted here again, that even though the THINC scheme is used for limiting the volume fraction, the other variables are limited using the vertex-based (VB) limiter, thus resulting in a THINC+VB limiting process. When the THINC limiter is not used, the VB limiter is used for all the flow variables.

5.1 Moving contact discontinuity problem

This test case is used to verify that the solver satisfies the pressure non-disturbance condition. It is also useful to judge the accuracy of the interface sharpening technique used. The following initial conditions are used:

$$(p, \alpha_g, u_k, T_k)_L = (10^5 \text{Pa}, 1 - \epsilon, 100 \text{m/s}, 300.0 \text{K})$$

$$(p, \alpha_g, u_k, T_k)_R = (10^5 \text{Pa}, \epsilon, 100 \text{m/s}, 300.0 \text{K})$$

$$\epsilon = 1.0 \times 10^{-7}$$

$$k = 1, 2$$

where the L and R states are to the left and right of $x = 0.5$ respectively. Fig. 1 shows the void-fraction and pressure obtained after running up to $t = 0.003$ using a $\Delta t = 10^{-6}$ on 200 cells. Profiles using the VB limiter and THINC+VB are shown together for comparison. It can be seen that the contact discontinuity is transported to the expected location and the uniform pressure is kept undisturbed. It is also observed that the THINC reconstruction for the volume fraction significantly improves the sharpness of the material interface. This can be clearly seen in Fig. 2, which shows the material interface closely. These results compare well with those by Nonomura et al. [32].

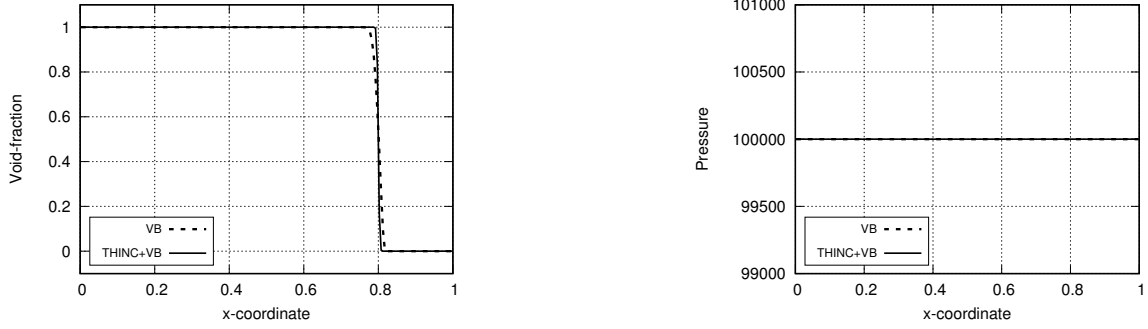


Figure 1: Void fraction (left) and Pressure (right) for the moving contact discontinuity

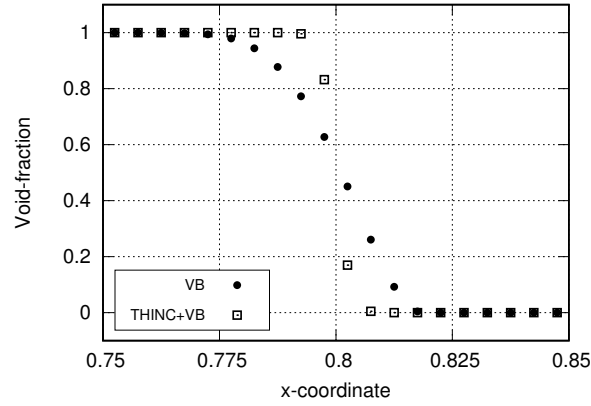


Figure 2: Comparison of the void fraction profiles with and without THINC reconstruction

5.2 Air/water shock-tube problem

This problem tests the capability of the method to capture shocks. It is a one-dimensional test case with the following initial conditions:

$$\begin{aligned}
 (p, \alpha_g, u_k, T_k)_L &= (10^9 \text{Pa}, 1 - \epsilon, 0 \text{m/s}, 308.15 \text{K}) \\
 (p, \alpha_g, u_k, T_k)_R &= (10^5 \text{Pa}, \epsilon, 0 \text{m/s}, 308.15 \text{K}) \\
 \epsilon &= 1.0 \times 10^{-7} \\
 k &= 1, 2.
 \end{aligned}$$

A mesh with 500 elements is used. The results at $t = 0.2 \times 10^{-3}$ using a $\Delta t = 5 \times 10^{-8}$, with and without THINC reconstruction are shown in Figs. 3 and 4. The results compare well with references [4, 6].

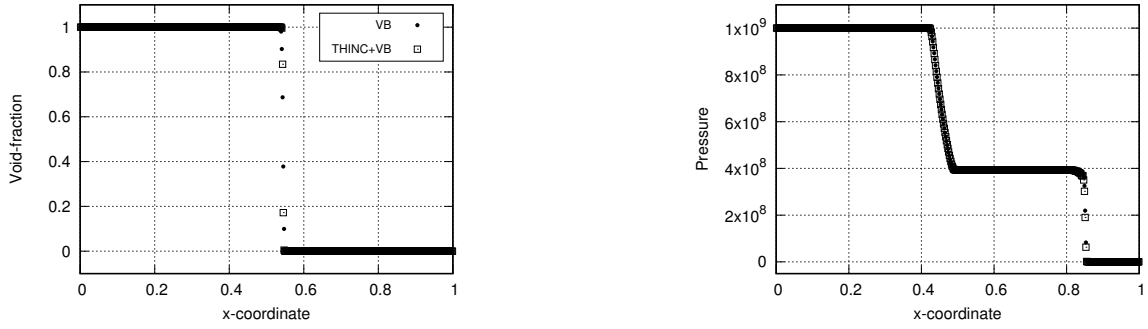


Figure 3: Void fraction (left) and Pressure (right) for the air-water shocktube

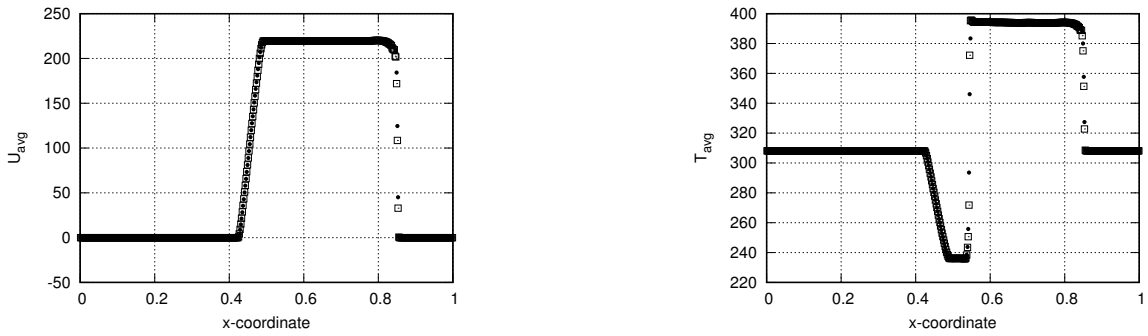


Figure 4: Average velocity (left) and temperature (right) for the air-water shocktube

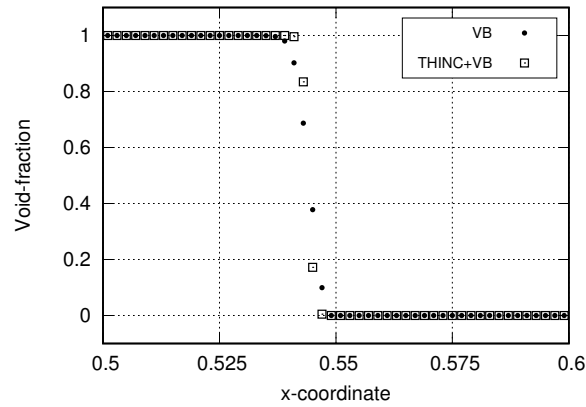


Figure 5: Comparison of the void fraction profiles for the air-water shocktube with and without THINC reconstruction

Fig. 5 shows the cell-averaged values of void fraction zoomed over particular regions to show the material interface. It can be seen that using THINC, the interface is captured in 4 cells as compared to 6 cells, when THINC is not used.

5.3 Water/air shock-tube problem

This is a one-dimensional test case with the following initial conditions:

$$\begin{aligned} (p, \alpha_g, u_k, T_k)_L &= (1.0 \times 10^8 \text{Pa}, \epsilon, 0 \text{m/s}, 308.15 \text{K}) \\ (p, \alpha_g, u_k, T_k)_R &= (1.0 \times 10^5 \text{Pa}, 1 - \epsilon, 0 \text{m/s}, 308.15 \text{K}) \\ \epsilon &= 1.0 \times 10^{-7} \\ k &= 1, 2. \end{aligned}$$

As mentioned by Kitamura et al. [6, 18], this high pressure-ratio water/air shocktube cannot be solved with the AUSM⁺ flux without augmenting an exact Riemann solver to it. However, the modifications in the AUSM⁺-upf flux allows this high pressure-ratio shocktube to be solved without the need for an exact Riemann solver. The results at $t = 0.2 \times 10^{-3}$ using a $\Delta t = 10^{-7}$, with and without THINC reconstruction are shown in Figs. 6 and 7. A mesh with 500 elements is used. The results show a good match with the references.

Fig. 8 shows the comparison of cell-averaged values of void fraction zoomed over particular regions to show the material interface. It can be seen that using THINC, the interface is captured in 3 cells instead of 5.

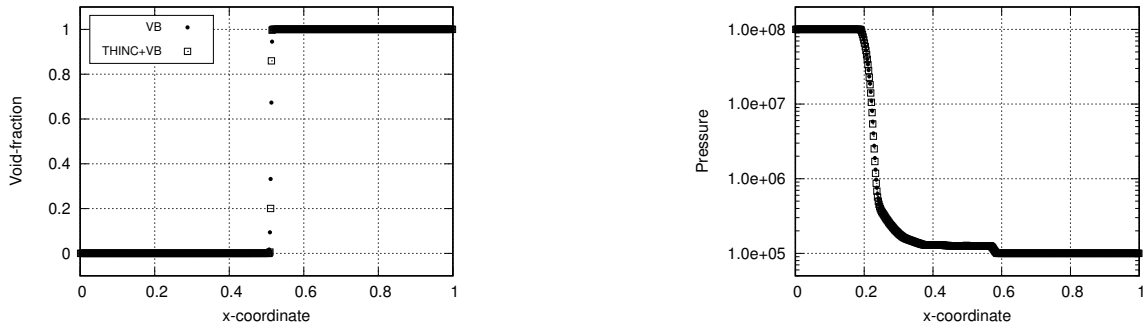


Figure 6: Void fraction (left) and Pressure (right) for the high PR water-air shocktube

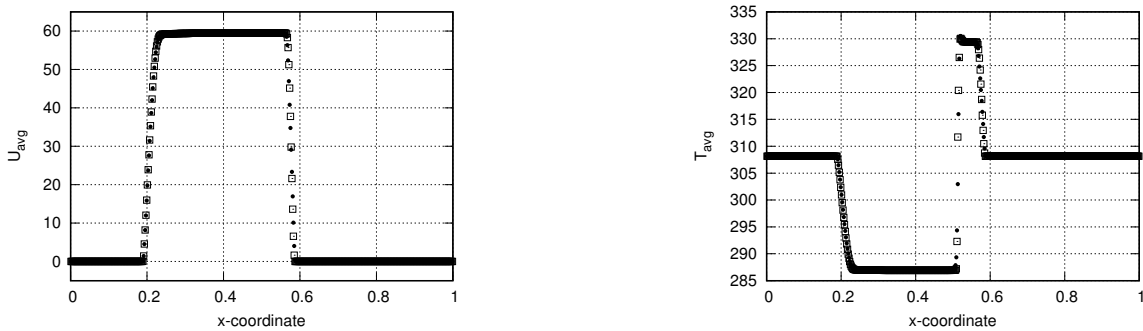


Figure 7: Average velocity (left) and temperature (right) for the high PR water-air shocktube

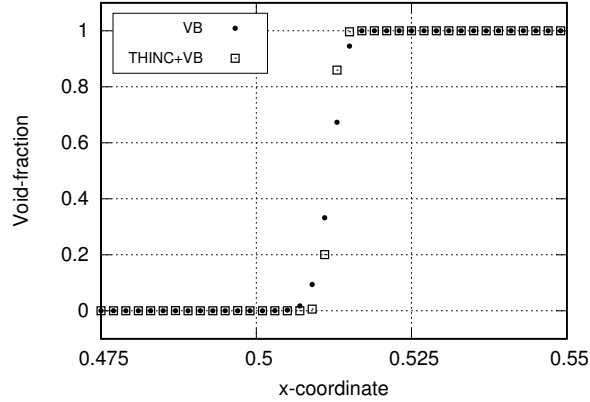


Figure 8: Comparison of the void fraction profiles for the water-air shocktube with and without THINC reconstruction

It has been previously noted that the pressure profiles obtained for this problem are especially sensitive to the flux scheme used [21, 22]. A grid convergence study was performed here for this reason. The THINC reconstruction is not used for this. Pressure profiles for meshes with 500, 1000 and 2000 elements are shown in Fig. 9, indicating that the method is indeed grid convergent.

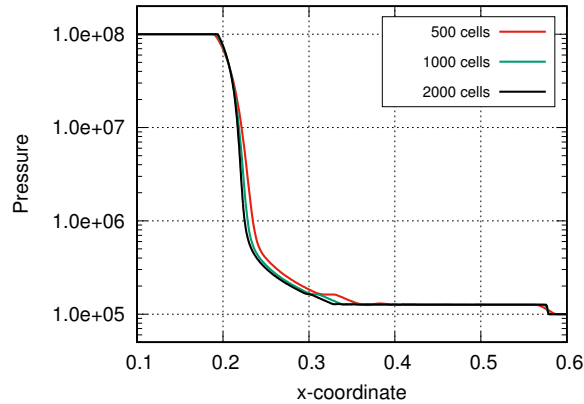


Figure 9: Pressure profiles showing grid-convergence for the high PR water-air shocktube

5.4 Shock/water-column interaction

A shock in air impacting a water-column (or a 2D droplet) is simulated in this problem. The droplet has radius $r = 3.2mm$ and is centered at the origin. Since this problem is symmetric about the X-axis, flow over only the top half of the droplet is simulated, and the symmetry condition is imposed at the bottom boundary. The droplet is resolved using 200×100 isotropic cells in the domain $[-5mm, 5mm] \times [0mm, 5mm]$, so that the grid spacing is $\Delta x_{min} = \Delta y_{min} = 0.05mm$ in this region. The rest of the grid is such that 450×150 total cells are used in the overall domain $[-15mm, 20mm] \times [0mm, 15mm]$. The initial conditions are [32]:

$$\begin{aligned}
 (p, \alpha_g, u_k, T_k)_L &= (2.35438 \times 10^5 \text{Pa}, \epsilon, 225.86m/s, 381.85\text{K}) \text{ for } x \leq 4mm \\
 (p, \alpha_g, u_k, T_k)_R &= (1.0 \times 10^5 \text{Pa}, \epsilon, 0m/s, 293.15\text{K}) \text{ for } x > 4mm, \text{ except for} \\
 &\quad x^2 + y^2 < (3.2mm)^2, \text{ where } \alpha_g = 1 - \epsilon \\
 \epsilon &= 1.0 \times 10^{-5} \\
 k &= 1, 2.
 \end{aligned}$$

These conditions result in a shock moving at $Ma = 1.47$, which impacts the droplet at $t \approx 1.5\mu s$. A time-step of $\Delta t = 1.25 \times 10^{-9}$ s is used.

A smooth transition of the volume fraction at the interface of the droplet is necessary. A width of $\pm 2\Delta x_{min}$ is used for the transition region. The curve used to fit the volume fraction in this region is the same as the blending function used for the vanishing phase.

$$\begin{aligned}\alpha_g|_{blended} &= G(\psi_2)\epsilon + (1 - G(\psi_2))(1 - \epsilon), \\ G(\psi_2) &= -\psi_2^2(2\psi_2 - 3), \\ \psi_2 &= \frac{\sqrt{x^2 + y^2} - (r - 2\Delta x_{min})}{4\Delta x_{min}}, \quad r - 2\Delta x_{min} \leq \sqrt{x^2 + y^2} \leq r + 2\Delta x_{min}.\end{aligned}$$

The left boundary is set as the inlet and the right boundary is the outlet. The top boundary is a slip-wall. These boundaries are sufficiently far from the droplet, such that their influence can be neglected.

The AUSM⁺-up fluxes (without the exact Riemann augmentation) diverge after $\approx 6.25\mu s$ of flow-time. However, if the AUSM⁺-upf fluxes are used, the method does not diverge at this point, and results at later flow-times can be obtained. Thus, only the results using AUSM⁺-upf are reported. Pressure and numerical Schlieren contours at $t = 6.25\mu s$, $t = 10\mu s$ and $t = 18.75\mu s$ are shown in Fig. 10 from top to bottom respectively. Pressure contours are plotted between 10^5 Pa and 4×10^5 Pa. The numerical Schlieren function is computed as $(1 + \alpha_l^2) \log(1 + |\nabla \rho|)$ and the range used for plotting its contours is 4 to 20. For this test problem, as the flow-time increases, the interface gets increasingly smeared. Hence, this example can be very useful in studying the effect of using THINC reconstruction. Fig. 11 shows numerical Schlieren and volume fraction plots using the VB limiter on the right, and THINC+VB limiter on the left, at flow-times $50\mu s$, $100\mu s$ and $200\mu s$ respectively. It can be clearly seen that using THINC keeps the interface very sharp, until the very end of the computation. This indicates that the THINC reconstruction for volume fraction is indeed very effective in retaining sharp interfaces. These results compare well with Nonomura et al. [32]

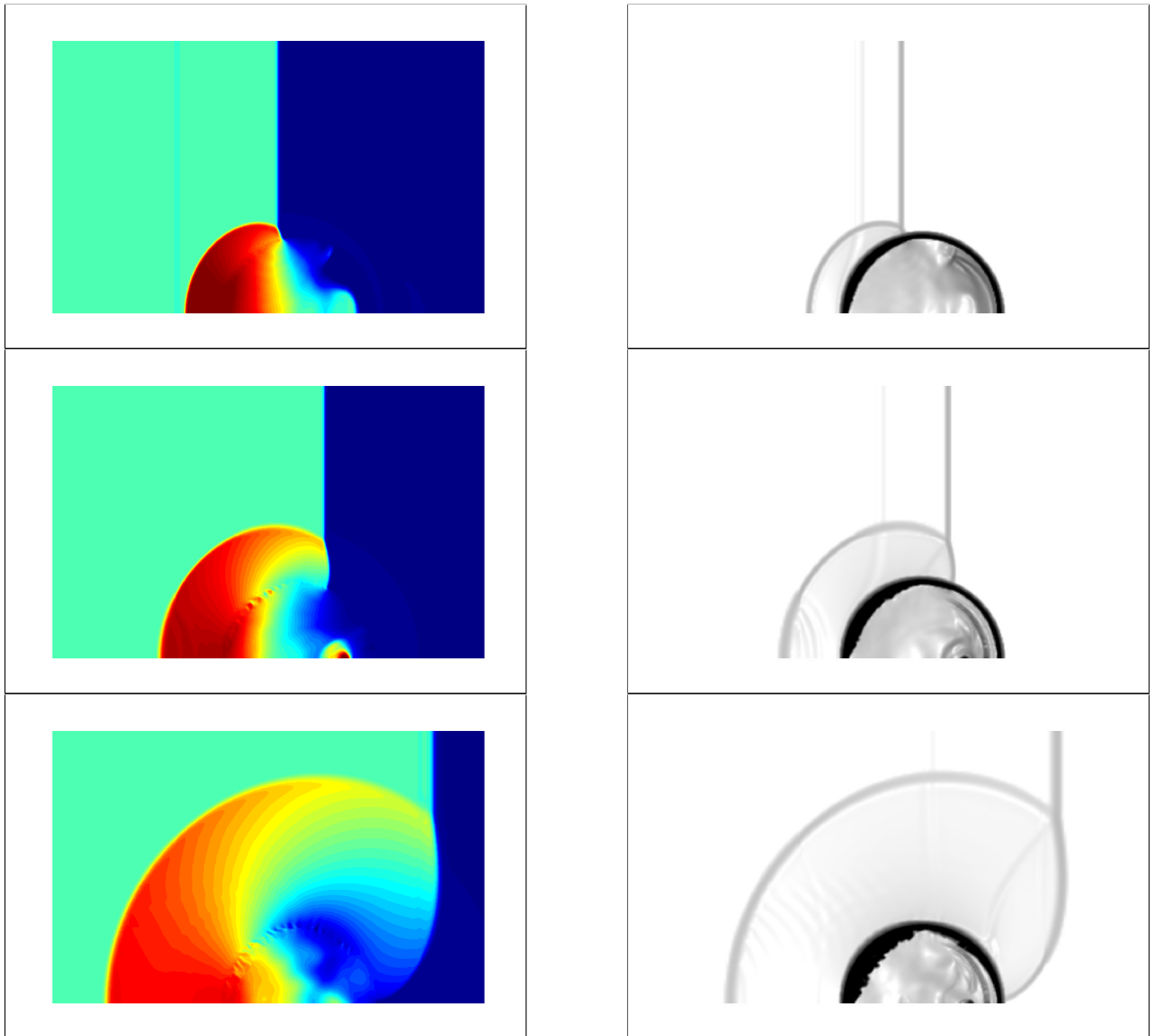


Figure 10: Pressure and numerical Schlieren contours for the shock/water-column interaction at $t = 6.25\mu s$, $10\mu s$ and $18.75\mu s$

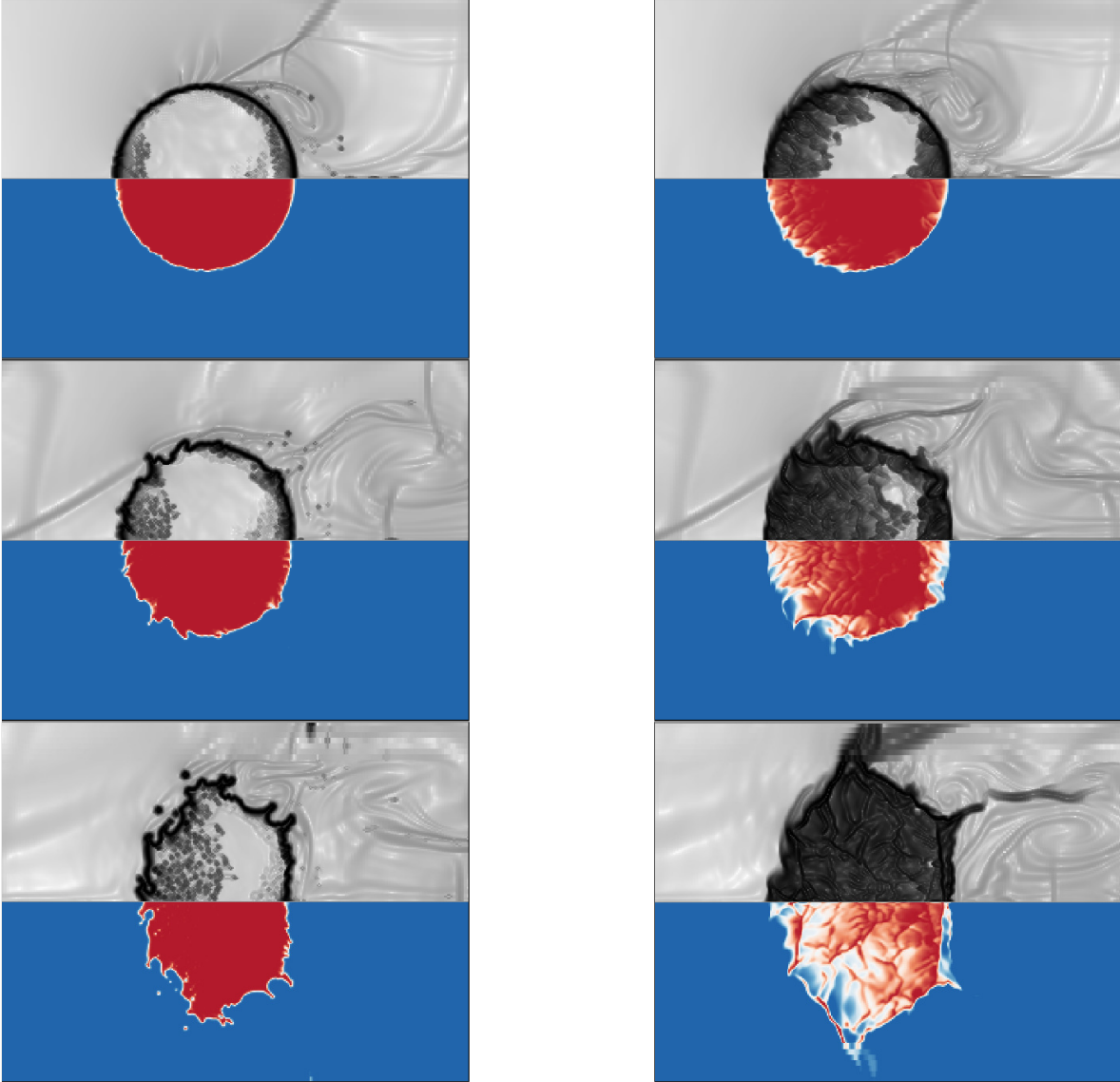


Figure 11: Numerical Schlieren (*top-half*) and volume fraction (*bottom-half*) contours for the shock/water-column interaction using THINC (*left*) and without using THINC reconstruction (*right*) at flow-times $t = 50\mu s$, $t = 100\mu s$ and $t = 200\mu s$

5.5 Shock/He-bubble interaction

This problem investigates the interface capturing capabilities of the proposed method. Shocks interacting with Helium bubbles and cylinders have been investigated experimentally by Haas and Sturtevant [44]. This problem has been solved computationally using the two-fluid model by Haimovich and Frankel [43] and using Lagrangian hydrodynamic methods by Burton et al. [45]. The experimental results above are used as a basis for comparison. The problem involves a Mach 1.22 shock impacting a Helium bubble with radius $2.5cm$. The problem is solved on a domain $[0m, 0.5m] \times [0m, 0.0445m]$, with the bubble centered at $(0.4, 0.0)$. A uniform mesh of 1200×160 elements is used, resulting in a $\Delta x = 0.42mm$ and $\Delta y = 0.28mm$. The initial

conditions are:

$$\begin{aligned}
(p, \alpha_g, u_k, T_k)_L &= (1.5698 \times 10^5 \text{Pa}, \epsilon, -113.5 \text{m/s}, 283.86 \text{K}) \text{ for } x \geq 0.45 \text{m} \\
(p, \alpha_g, u_k, T_k)_R &= (1.01325 \times 10^5 \text{Pa}, \epsilon, 0 \text{m/s}, 248.88 \text{K}) \text{ for } x < 0.45 \text{m, except for} \\
&\quad (x - 0.4)^2 + y^2 < (0.025 \text{m})^2, \text{ where } \alpha_g = 1 - \epsilon \\
&\quad \epsilon = 1.0 \times 10^{-5} \\
&\quad k = 1, 2.
\end{aligned}$$

The same smooth transition over 2 cells for the material interface like the one used in the previous shock-bubble problems is used here as well. The THINC reconstruction has been used for this problem. Without THINC, the bubble interface gets smeared out beyond recognition. Thus, the results without using THINC are not included.

The numerical Schlieren and volume fraction contours of Helium at times $80 \mu\text{s}$, $240 \mu\text{s}$, $420 \mu\text{s}$, $680 \mu\text{s}$ and $980 \mu\text{s}$ are shown in Fig. 12, as compared to the experimental results of Haas and Sturtevant [44]. These times, as noted in the reference, are after the shock hits the bubble. The numerical results compare well with the experiments. It should be noted that at the final time $980 \mu\text{s}$, the bubble has already collapsed onto itself. However, the THINC limiting enables accurate interface capturing even in this situation. It is also noteworthy that the mesh used in this problem is significantly coarser as compared to the meshes conventionally used by Eulerian methods. The purpose of using a coarser mesh is to demonstrate that the shock-interface interaction can be accurately computed nevertheless.

5.6 Shock/R22-bubble interaction

This problem is also used to demonstrate the interface capturing capabilities of the proposed method. Experimental results of shocks interacting with R22 bubbles and cylinders can also be found in the work by Haas and Sturtevant [44]. Computational results for this problem have been presented using the two-fluid model by Nonomura and Kitamura [32]. The problem involves a Mach 1.22 shock impacting an R22 bubble with radius 2.5cm , centered at $(0.225, 0.0)$. The same mesh-setup as the previous problem is used here. The initial conditions are:

$$\begin{aligned}
(p, \alpha_g, u_k, T_k)_L &= (1.59 \times 10^5 \text{Pa}, \epsilon, -113.5 \text{m/s}, 328.6 \text{K}) \text{ for } x \geq 0.275 \text{m} \\
(p, \alpha_g, u_k, T_k)_R &= (1.01325 \times 10^5 \text{Pa}, \epsilon, 0 \text{m/s}, 288.2 \text{K}) \text{ for } x < 0.275 \text{m, except for} \\
&\quad (x - 0.225)^2 + y^2 < (0.025 \text{m})^2, \text{ where } \alpha_g = 1 - \epsilon \\
&\quad \epsilon = 1.0 \times 10^{-5} \\
&\quad k = 1, 2.
\end{aligned}$$

The same smooth transition for the material interface over 2 cells is used. Numerical results using the THINC reconstruction are presented here, because the interface is smeared out when THINC is not used. Numerical Schlieren functions and R-22 volume fractions are shown at times $50 \mu\text{s}$, $250 \mu\text{s}$, $420 \mu\text{s}$ and $1020 \mu\text{s}$ in Fig. 13 as compared to experiments from Haas and Sturtevant. The numerical results show good comparison with the experiments, in spite of using a coarse mesh. This emphasizes the effect of the THINC interface sharpening technique on the two-fluid model.

5.7 Underwater detonation

This test simulates detonation conditions under water, and its effects on the water surface. A rectangular domain $10 \text{m} \times 14 \text{m}$ is initialized with water 3.5m deep. The top, right and bottom boundaries are extrapolated and the left boundary is symmetric. A sphere with radius 0.3m containing high pressure air is placed with

it's center $0.5m$ under the water surface. The initial conditions inside the sphere are:

$$\begin{aligned}(p, \alpha_g, u_k, T_k) &= (10^9 \text{Pa}, 1.0 - \epsilon, 0.0 \text{m/s}, 2000.0 \text{K}) \\ \epsilon &= 1.0 \times 10^{-3} \\ k &= 1, 2\end{aligned}$$

and the pressure and temperature everywhere else are 300K and $1.01325 \times 10^5 \text{Pa}$ respectively. An unstructured mesh with 115,000 elements is used to discretize the domain, and a time-step of $\Delta t = 2.5 \times 10^{-7}$ is used for this problem. A smooth transition of the volume fraction is used for the water surface and the surface of the sphere. Numerical results at 1 ms, 4 ms, and 6 ms using the THINC reconstruction are shown in Fig. 14. At 6 ms, it is apparent that the mesh resolution is insufficient to capture the splashed water separating into smaller fragments. Nevertheless, the sharp interface resolution of the THINC reconstruction is clear from these results.

6 Conclusion

A robust and efficient modification to the AUSM⁺-up flux in the context of non-equilibrium two-fluid flows has been presented. The regular AUSM⁺-up suffers from negative middle-zone pressures in regions where strong shocks interact with material interfaces. The presented enhancement is shown to make the method robust in such situations. Since the modifications do not involve any iterative procedure like the exact Riemann solver, in addition to being robust, the resulting discretization has a low computational cost. Further, the multidimensional THINC interface sharpening technique is used in conjunction with the proposed discretization of the two-fluid single pressure model. It is shown that the material interface is captured very sharply using THINC as compared to a conventional TVD limiter. A number of numerical experiments involving shock-bubble interactions have been considered to assess the robustness and the interface capturing capability of the developed finite volume method for inviscid two-phase flow problems. The numerical results demonstrate that the robustness is indeed enhanced by the modifications made in the flux function. When used in conjunction with the THINC scheme, the modified AUSM⁺-up flux function shows great potential to be able to efficiently solve challenging shocked two-phase flow problems.

Acknowledgments

This research was partially supported by the Consortium for Advanced Simulation of Light Water Reactors (<http://www.casl.gov>), an Energy Innovation Hub (<http://www.energy.gov/hubs>) for Modeling and Simulation of Nuclear Reactors under U.S. Department of Energy Contract No. DE-AC05-00OR22725. The authors would like to thank Dr. C. -H. Chang, Dr. N. Dinh, Dr. J. R. Edwards, and Dr. R. Nourgaliev for fruitful discussions.

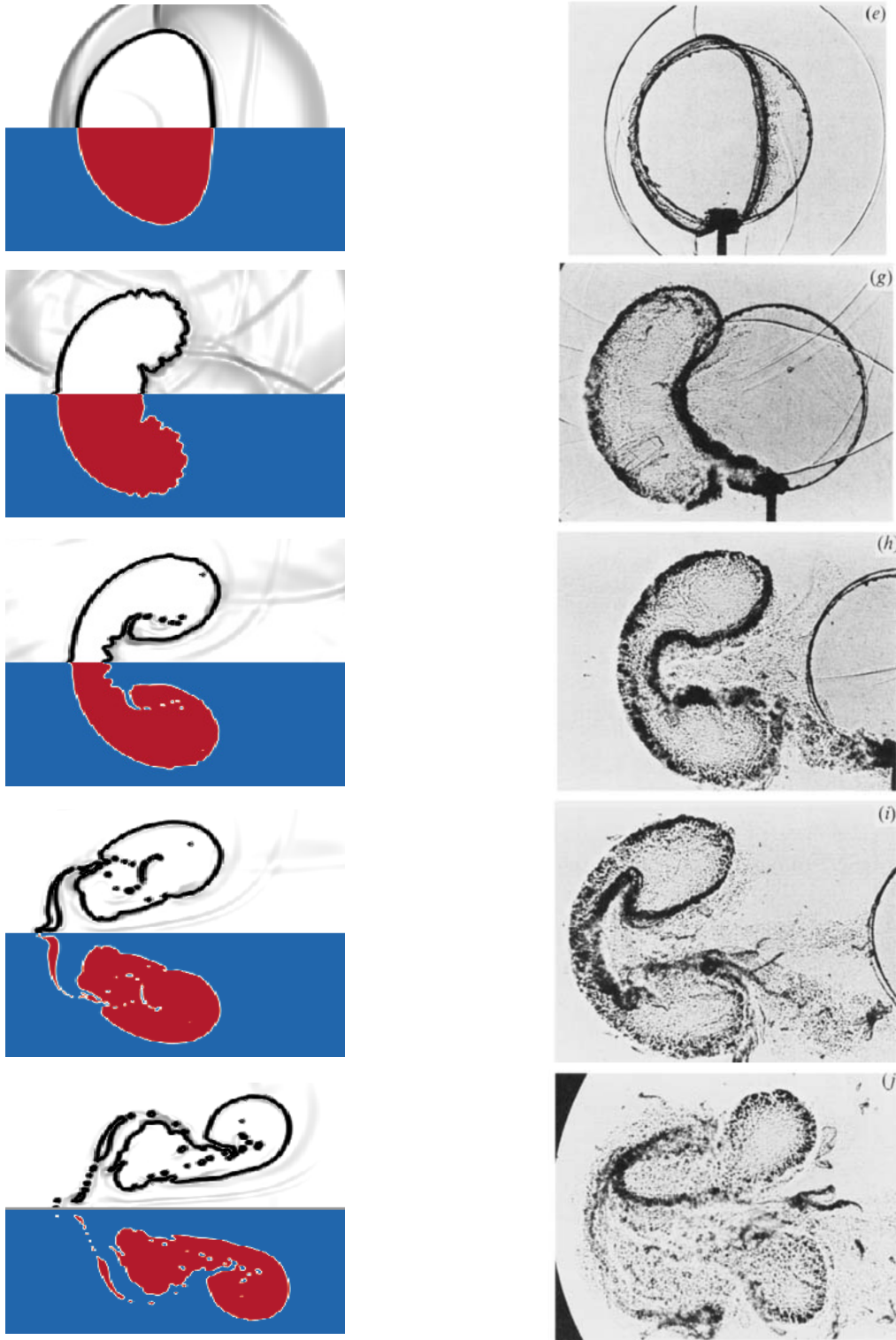


Figure 12: Numerical Schlieren (*top-half*) and volume-fraction (*bottom-half*) contours for the shock-He cylinder interaction test at $t = 80 \mu s, 240 \mu s, 420 \mu s, 680 \mu s$ and $980 \mu s$. THINC (*left-column*) compared to experiments from Haas and Sturtevant (1987) [44] (*right-column*)

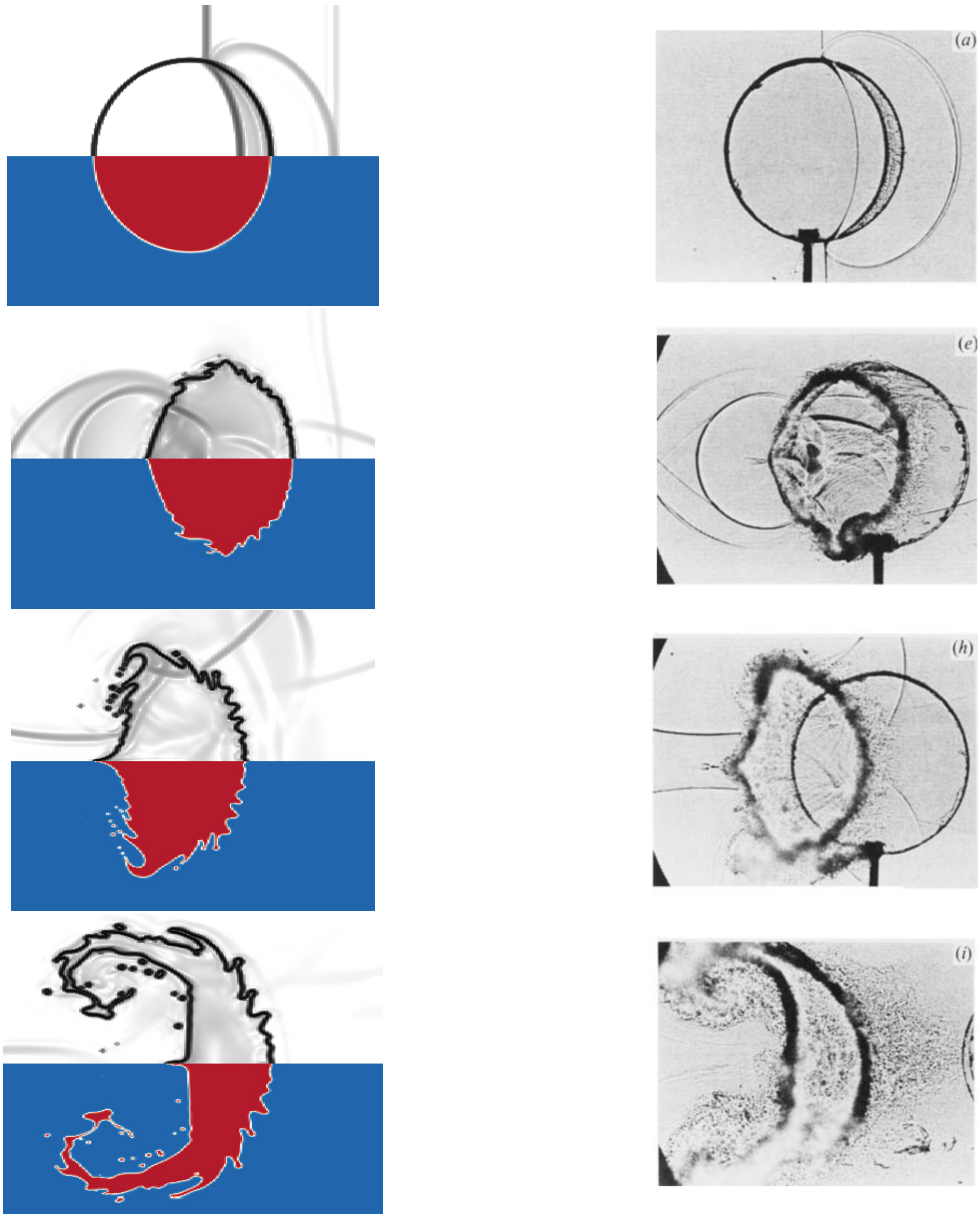


Figure 13: Numerical Schlieren (*top-half*) and volume-fraction (*bottom-half*) contours for the shock-R22 cylinder interaction test (*left-column*) at $t = 50\mu s, 250\mu s, 420\mu s, 1020\mu s$ compared to experiments from Haas and Sturtevant (1987) [44] (*right-column*)

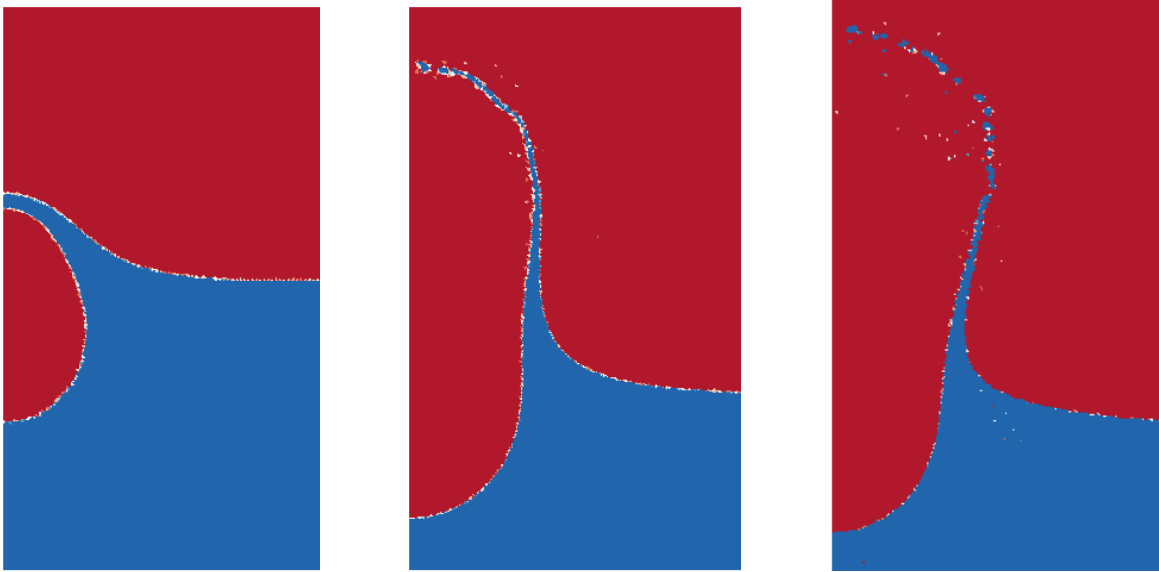


Figure 14: Volume-fraction contours for the underwater detonation test at $t = 1ms, 4ms,$ and $6ms$

References

- [1] M Ishii and T Hibiki. *Thermo-fluid dynamics of two-phase flow*. Springer Science & Business Media, 2010.
- [2] G B Wallis. *One-dimensional two-phase flow*. McGraw-Hill Companies, 1969.
- [3] I Toumi and A Kumbaro. An approximate linearized riemann solver for a two-fluid model. *Journal of Computational Physics*, 124(2):286–300, 1996.
- [4] C-H Chang and M-S Liou. A robust and accurate approach to computing compressible multiphase flow: Stratified flow model and AUSM+-up scheme. *Journal of Computational Physics*, 225(1):840–873, 2007.
- [5] M-S Liou, C-H Chang, L Nguyen, and T G Theofanous. How to solve compressible multifluid equations: a simple, robust, and accurate method. *AIAA Journal*, 46(9):2345–2356, 2008.
- [6] K Kitamura, M-S Liou, and C-H Chang. Extension and comparative study of AUSM-family schemes for compressible multiphase flow simulations. *Communications in Computational Physics*, 16(03):632–674, 2014.
- [7] D Lhuillier, C-H Chang, and T G Theofanous. On the quest for a hyperbolic effective-field model of disperse flows. *Journal of Fluid Mechanics*, 731:184–194, 2013.
- [8] Y-Y Niu. Computations of two-fluid models based on a simple and robust hybrid primitive variable Riemann solver with AUSMD. *Journal of Computational Physics*, 308:389–410, 2016.
- [9] Y-Y Niu and H-W Wang. Simulations of the shock waves and cavitation bubbles during a three-dimensional high-speed droplet impingement based on a two-fluid model. *Computers & Fluids*, 134:196–214, 2016.
- [10] TN Dinh, RR Nourgaliev, and TG Theofanous. Understanding the ill-posed two-fluid model. In *Proceedings of the 10th international topical meeting on nuclear reactor thermal-hydraulics (NURETH-10)*, 2003.
- [11] RR Nourgaliev, TN Dinh, and TG Theofanous. A characteristics-based approach to the numerical solution of the two-fluid model. In *ASME/JSME 2003 4th Joint Fluids Summer Engineering Conference*, pages 1729–1748. American Society of Mechanical Engineers, 2003.
- [12] T Vazquez-Gonzalez, A Llor, and C Fochesato. Ransom test results from various two-fluid schemes: Is

- enforcing hyperbolicity a thermodynamically consistent option? *International Journal of Multiphase Flow*, 81:104–112, 2016.
- [13] MR Baer and JW Nunziato. A two-phase mixture theory for the deflagration-to-detonation transition (DDT) in reactive granular materials. *International Journal of Multiphase Flow*, 12(6):861–889, 1986.
- [14] R Saurel and R Abgrall. A simple method for compressible multifluid flows. *SIAM Journal on Scientific Computing*, 21(3):1115–1145, 1999.
- [15] R Saurel and R Abgrall. A multiphase Godunov method for compressible multifluid and multiphase flows. *Journal of Computational Physics*, 150(2):425–467, 1999.
- [16] R Saurel and O Lemetayer. A multiphase model for compressible flows with interfaces, shocks, detonation waves and cavitation. *Journal of Fluid Mechanics*, 431:239–271, 2001.
- [17] Rémi Abgrall and Richard Saurel. Discrete equations for physical and numerical compressible multiphase mixtures. *Journal of Computational Physics*, 186(2):361–396, 2003.
- [18] K Kitamura and T Nonomura. Simple and robust HLLC extensions of two-fluid AUSM for multiphase flow computations. *Computers & Fluids*, 100:321–335, 2014.
- [19] M-S Liou. A sequel to AUSM, part II: AUSM+–up for all speeds. *Journal of Computational Physics*, 214(1):137–170, 2006.
- [20] RW Houim and ES Oran. A multiphase model for compressible granular–gaseous flows: formulation and initial tests. *Journal of Fluid Mechanics*, 789:166–220, 2016.
- [21] A Pandare and H Luo. A finite volume method for compressible viscous multiphase flows. In *2018 AIAA Aerospace Sciences Meeting*, page 1814, 2018.
- [22] A K Pandare and H Luo. A robust and efficient finite volume method for compressible inviscid and viscous two-phase flows. *Journal of Computational Physics*, 371:67–91, 2018.
- [23] R Abgrall. How to prevent pressure oscillations in multicomponent flow calculations: a quasi conservative approach. *Journal of Computational Physics*, 125(1):150–160, 1996.
- [24] C Parés. Numerical methods for nonconservative hyperbolic systems: a theoretical framework. *SIAM Journal on Numerical Analysis*, 44(1):300–321, 2006.
- [25] F Xiao, Y Honma, and T Kono. A simple algebraic interface capturing scheme using hyperbolic tangent function. *International Journal for Numerical Methods in Fluids*, 48(9):1023–1040, 2005.
- [26] B Xie, S Li, and F Xiao. An efficient and accurate algebraic interface capturing method for unstructured grids in 2 and 3 dimensions: The thinc method with quadratic surface representation. *International Journal for Numerical Methods in Fluids*, 76(12):1025–1042, 2014.
- [27] A Chiapolino, R Saurel, and B Nkonga. Sharpening diffuse interfaces with compressible fluids on unstructured meshes. *Journal of Computational Physics*, 340:389–417, 2017.
- [28] Herbert Städtke. *Gasdynamic aspects of two-phase flow: Hyperbolicity, wave propagation phenomena and related numerical methods*. John Wiley & Sons, 2006.
- [29] JH Stuhmiller. The influence of interfacial pressure forces on the character of two-phase flow model equations. *International Journal of Multiphase Flow*, 3(6):551–560, 1977.
- [30] Chih-Hao Chang, Svetlana Sushchikh, Loc Nguyen, Meng-Sing Liou, and Theo Theofanous. Hyperbolicity, discontinuities, and numerics of the two-fluid model. In *5th ASME/JSME Fluids Engineering Summer Conference, 10th International Symposium on Gas-Liquid Two-phase Flows*. San Diego, 2007.
- [31] Dmitri Kuzmin. A vertex-based hierarchical slope limiter for p-adaptive discontinuous Galerkin methods. *Journal of computational and applied mathematics*, 233(12):3077–3085, 2010.
- [32] T Nonomura, K Kitamura, and K Fujii. A simple interface sharpening technique with a hyperbolic tangent function applied to compressible two-fluid modeling. *Journal of Computational Physics*, 258:95–117, 2014.
- [33] Satoshi Ii, Bin Xie, and Feng Xiao. An interface capturing method with a continuous function: The thinc method on unstructured triangular and tetrahedral meshes. *Journal of Computational Physics*, 259:260–269, 2014.
- [34] J-M Hérard and O Hurisse. A simple method to compute standard two-fluid models. *International Journal of Computational Fluid Dynamics*, 19(7):475–482, 2005.
- [35] T Gallouët, P Helluy, J-M Hérard, and J Nussbaum. Hyperbolic relaxation models for granular flows. *ESAIM: Mathematical Modelling and Numerical Analysis*, 44(2):371–400, 2010.
- [36] M-S Liou and J R Edwards. Numerical speed of sound and its application to schemes for all speeds. In *14th Computational Fluid Dynamics Conference*, page 3268, 1999.

- [37] J R Edwards. Towards unified CFD simulations of real fluid flows. In *15th AIAA Computational Fluid Dynamics Conference*, page 2524, 2001.
- [38] MJ Castro, ED Fernández-Nieto, AM Ferreiro, JA García-Rodríguez, and C Parés. High order extensions of Roe schemes for two-dimensional nonconservative hyperbolic systems. *Journal of Scientific Computing*, 39(1):67–114, 2009.
- [39] M Dumbser and EF Toro. A simple extension of the Osher Riemann solver to non-conservative hyperbolic systems. *Journal of Scientific Computing*, 48(1):70–88, 2011.
- [40] ST Munkejord, S Evje, and T Flåtten. A musta scheme for a nonconservative two-fluid model. *SIAM Journal on Scientific Computing*, 31(4):2587–2622, 2009.
- [41] Sigal Gottlieb and Chi-Wang Shu. Total variation diminishing Runge-Kutta schemes. *Mathematics of computation of the American Mathematical Society*, 67(221):73–85, 1998.
- [42] H Paillere, C Corre, and JR Garcia Cascales. On the extension of the AUSM+ scheme to compressible two-fluid models. *Computers & Fluids*, 32(6):891–916, 2003.
- [43] O Haimovich and S H Frankel. Numerical simulations of compressible multicomponent and multiphase flow using a high-order targeted eno (teno) finite-volume method. *Computers & Fluids*, 146:105–116, 2017.
- [44] J-F Haas and B Sturtevant. Interaction of weak shock waves with cylindrical and spherical gas inhomogeneities. *Journal of Fluid Mechanics*, 181:41–76, 1987.
- [45] D E Burton, N R Morgan, T C Carney, and M A Kenamond. Reduction of dissipation in lagrange cell-centered hydrodynamics (CCH) through corner gradient reconstruction (CGR). *Journal of Computational Physics*, 299:229–280, 2015.